Development of Robust Metal-Supported SOFCs and Stack Components in EU METSAPP Consortium

Sudireddy, Bhaskar Reddy; Nielsen, Jimmi; Persson, Åsa Helen; Thydén, Karl Tor Sune; Brodersen, Karen; Ramousse, Severine; Neagu, D.; Stefan, E.; Irvine, J. T. S.; Geisler, H.

Total number of authors:
23

Published in:
Fuel Cells

Link to article, DOI:
10.1002/fuce.201600191

Publication date:
2017

Document Version
Peer reviewed version

Development of Robust Metal-Supported SOFCs and Stack Components in EU-METSAPP Consortium

Journal:	*Fuel Cells*
Manuscript ID	fuce.201600191.R1
Wiley - Manuscript type:	Original Research Paper
Date Submitted by the Author:	n/a
Complete List of Authors:	Sudireddy, Bhaskar Reddy; Technical University of Denmark, Department of Energy Conversion and Storage Nielsen, Jimmi Persson, Åsa Thydén, Karl Brodersen, Karen Ramousse, Severine Neagu, Dragos Stefan, Elena Irvine, John Geisler, Helge Weber, André Reiss, Georg Schauperl, Richard Rechberger, J Froitzheim, Jan Sachitanand, R Falk-Windisch, H Svensson, J Lundburg, M Berger, R Westlinder, J Hornauer, S Kiefer, T
Keywords:	Degradation, Electrochemistry, Energy conversion, Fuel cell stacks, Metal-supported solid oxide cells, Modelling, Nanostructured protective coatings, Strontium titanate

Development of Robust Metal-Supported SOFCs and Stack Components in EU-METSAPP Consortium

B.R. Sudireddy[*,1], J. Nielsen[1], Å. H. Persson[1], K. Thydén[1], K. Brodersen[1], S. Ramousse[1], D. Neagu[2], E. Stefan[2], J.T.S. Irvine[2], H. Geisler[3], A. Weber[3], G. Reiss[4,a], R. Schauperl[5], J. Rechberger[5], J. Froitzheim[6], R. Sachitanand[6], H. Falk-Windisch[6], J. E. Svensson[6], M. W. Lundberg[7], R. Berger[7], J. Westlinder[7], S. Hornauer[8], T. Kiefer[8]

[1] Department of Energy Conversion and Storage, Technical University of Denmark Frederiksborgvej 399, DK-4000, Roskilde, Denmark
[2] School of Chemistry, University of St Andrews, St Andrews, Fife KY16 9ST, Scotland, UK
[3] Institute for Applied Materials (IAM-WET), Karlsruhe Institute of Technology (KIT), D-76131 Karlsruhe, Germany
[4] ICE Strömungsforschung GmbH, Hauptplatz 13, 8700 Leoben, Austria
[5] AVL List GmbH, Hans-List-Platz 1, A-8020 Graz, Austria
[6] Department of Chemistry and Chemical Engineering, Chalmers University of Technology, 41296 Gothenburg, Sweden
[7] AB Sandvik Materials Technology, SFFY (4371), SE-811 81 Sandviken, Sweden
[8] ElringKlinger AG, Max-Eyth-Stasse 2, 72581 Dettingen, Germany

[a] Currently at MCL Forschung GmbH, Roseggerstraße 12, 8700 Leoben, Austria
[*] Corresponding author: bhsu@dtu.dk

Abstract:

The potential of MS-SOFCs was demonstrated through the previous EU METSOFC project, which concluded that the development of corrosion resistant novel MS-SOFC design and stack is the requirement to advance this technology to the next level. The following EU METSAPP project has been executed with an overall aim of developing advanced metal-supported cells and stacks based on a robust, reliable and up-scalable technology. During the project, corrosion resistant nanostructured anodes based on modified $SrTiO_3$ were developed and integrated into MS-SOFCs to enhance their robustness. In addition, the manufacturing of metal-supported cells with different geometries, scalability of the manufacturing process was demonstrated and more than 200 cells with an area of ≈150 cm^2 were produced. The electrochemical performance of different cell generations was evaluated and best performance and stability combination was observed with doped-$SrTiO_3$ based anode designs. Furthermore, numerical models to understand the corrosion behavior of the MS-SOFCs were developed and validated. Finally, the cost effective concept of coated metal interconnects was developed, which resulted in 90% reduction in Cr evaporation, three times lower Cr_2O_3 scale thickness and increased lifetime. The possibility of assembling these cells into two radically different stack designs was demonstrated.

Keywords: Degradation, Electrochemistry, Energy conversion, Fuel cell stacks, Metal-supported solid oxide cells, Modelling, Nanostructured protective coatings, Strontium titanate

1. Introduction

Solid oxide fuel cells (SOFCs) are high temperature electrochemical devices that convert chemical energy into electrical energy. The relatively high energy conversion efficiency compared to conventional devices makes the SOFC technology very attractive. However, cost and limited durability are the major challenges restraining the introduction of SOFCs into the commercial market. The metal-supported solid oxide fuel cell (MS-SOFC) has a relatively low operating temperature compared to conventional SOFC and is a promising technology with respect to the above-mentioned challenges. Along with the reduction of material cost, the MS-SOFCs offer higher robustness due to the ductility and higher thermal conductivity of the metal-support. These physical properties provide high tolerance to thermal cycling, redox cycling, and shock vibrations, which are beneficial for auxiliary power units (APUs) and other mobile applications [1,2].

In spite of the above-mentioned advantages, there is a significant need to develop stable and high performing electrodes for the MS-SOFCs, particularly the anode. The use of conventional Ni and Y_2O_3 stabilized ZrO_2 (Ni-YSZ) cermet based anode functional layer (AFL) in metal-supported cells leads to problems such as Ni inter-diffusion into the metal-support and as a result poor redox stability [2,3]. One of the solutions to avoid such problems is the use of Ni-free anode backbone materials. However, such cell designs require the additional integration of electrocatalytically active materials into the anode backbone to make the electrode fully functional.

In the previous EU METSOFC project, anode designs based on ferritic stainless steel (FeCr) -YSZ with Ni:GDC (Gd doped CeO_2 (GDC) with small amount of Ni) electrocatalyst were developed successfully and these AFL designs demonstrated significantly improved electrochemical performance [4-6]. However, going to more realistic operating conditions i.e., reformates and high fuel utilization, higher degradation rates were observed due to the severe oxidation of FeCr metal phase in the AFL [7]. This necessitates the development of oxidation resistant and stable performing anodes for MS-SOFCs. Furthermore, understanding of degradation mechanisms and modelling of the degradation phenomena for the conventional SOFCs based on Ni-YSZ has progressed significantly; however, similar understanding for the MS-SOFCs is scarce. It is imperative to identify the main degradation mechanisms for MS-SOFCs in order to achieve commercialization of this technology. In addition, to demonstrate the economic and technological

potential of the MS-SOFC technology, the development of up-scalable cell fabrication technology for the largest possible cell footprint area is needed. Furthermore, in order to mature the MS-SOFC stack technology, well-optimized stack designs and stable stack components are required. Keeping the above-mentioned challenges and requirements in focus, the activities in the EU METSAPP project are centered on the development of high performing oxidation resistant cells, scalable cell manufacturing process, robust stack components, stack designs and building of robust stacks utilizing different characterization tools and numerical models. We report here an overview of the most important advancements achieved during the course of the project with respect to the above-mentioned aspects. More details about the project and the consortium members can be found at www.metsapp.eu.

2 Results and Discussion

2.1 Cell Development and Manufacturing

The design of the MS-SOFC and the cell fabrication process that were developed in EU METSOFC project were continued to be used in the EU METSAPP project, the details of which were described in refs. [2,8]. The MS-SOFC components, i.e., metal-support, anode backbone and electrolyte were co-casted using tape casting. This group of components (half-cell) was co-sintered in reducing atmosphere. A barrier layer was applied on the electrolyte using a physical vapor deposition (PVD) method before applying the cathode layer using screen-printing. After the cathode printing, the electrocatalyst materials (GDC with small amount of Ni metal) were integrated into the anode backbone using precursor salt solution impregnation technique. The cathode layer was sintered in-situ during the initialization of cell testing / stack conditioning. This sequence of processes for cell development and fabrication was maintained throughout the project with minor modifications.

The development of robust oxidation resistant cells was approached through different strategies. The main strategies were: 1) Improving the oxidation resistance of the FeCr-YSZ based AFL, developed in EU METSOFC project, using protective coatings, 2) replacing the FeCr-YSZ based AFL with novel electrode materials, and 3) development and integration of high performance cathodes. The details of which are presented in sections below. The cells with FeCr-YSZ AFL were denoted as Type A cells and the cells with novel electrode materials were denoted as Type B cells for the ease of identification. The developments made concerning the cathodes were implemented in both type of cells. All the other components, namely metal-support, electrolyte and barrier layer, were kept the same in both type of cells.

2.1.1 Development of Protective Nanostructured Coatings

In this approach, protective coatings were developed for Type A cells. The primary function of the coating was to limit the oxidation of the FeCr-YSZ based AFL by limiting the formation of Cr_2O_3 on FeCr particles. The coating was also expected to move the reaction zone away from the FeCr surface to lower the accelerated oxide formation upon drawing a current [9].

Different coating materials such as reactive elements, chromites, titanates, metal oxides and spinels were investigated for their efficiency in improving the oxidation resistance in relevant conditions. The titanate based coatings such as doped $SrTiO_3$ and doped TiO_2 were either difficult to form at low temperature (below 1000°C) or unstable in MS-SOFC operating conditions. Metal oxide coatings such as CuO were successfully formed at lower temperatures (< 400°C). However, the CuO was reduced to Cu and the coating was disintegrated into discrete particles in the fuel electrode environment [10], which resulted in an inefficient protection of FeCr surfaces. The other coating materials i.e., reactive elements, chromites and spinels were the most promising. The major challenge with these materials was obtaining a continuous and uniform coating on the FeCr porous structures. The quality of the obtained coatings was strongly dependent on the impurities on metal surface and the wettability of the coating precursor solutions. Figure 1 shows the spinel coatings obtained on the porous metal-supports with different surface quality. It can be clearly seen from Figure 1a that the surface contamination, in this case Si, resulted in an intermediate contaminated layer between metal surface and spinel coating that could influence the adhesion of the coating. The clean metal surface shows no intermediate layers between the metal surface and spinel coating and good adhesion with the metal surface (Figure 1b). However, it can also be noticed the thickness of the coating is not uniform across all the metal surfaces. Thus, the adherence and uniformity of these coatings requires further optimization to completely realize their potential in improving the oxidation resistance of metal surfaces.

2.1.2 Development of Alternative Anode Designs

In this approach, efforts were made to replace the FeCr-YSZ based AFL with an alternative electrode material to develop Type B cells. The alternative anode designs were based on electronically conducting ceramic materials such as doped $SrTiO_3$. These materials should be stable under highly reducing environment at high temperatures during cell processing, possess good electronic conductivity and compatible with other cell components. Among the doped $SrTiO_3$

materials, Nb-doped $SrTiO_3$ (STN) and (La,Sr)(Ti,Fe,Ni)O_3 (LSFNT) materials were extensively investigated either as a single material or as a composite with other materials, predominantly FeCr. The electrochemical performance of the STN-FeCr composite based anode designs was inferior; however, the oxidation resistance was significantly improved when compared to FeCr-YSZ designs. Introducing STN as a composite with the FeCr phase in the anode backbone led to a decrease in the formation of Cr_2O_3 on the FeCr particles. STN seem to block the inward diffusion of oxygen ions (if it covers the FeCr surface) [11]. However, Cr diffusion seems to occur at STN grain boundaries and allows for the Cr-rich oxides formation in the pores of the anode and electrolyte. The main challenge observed with STN based AFLs was their integration in to the current MS-SOFC design due to their different sintering behaviour in cell processing conditions, resulting in poor adhesion with electrolyte and leaky electrolyte layer (Figure 2a).

The LSFNT anode backbone showed the most promising characteristics required for their integration into MS-SOFCs. The special characteristic of these materials, exsolution of the nanoparticles [12], contributed to the improved adhesion with other cell components and probably enhanced their electrochemical performance. These materials possess satisfying electrical transport properties and favourable sintering behaviour to be matched with other cell materials, making their integration into the MS-SOFCs successful. Different anode backbone designs were formulated using this material to optimize the cells. These anode backbone designs consist of LSFNT, LSFNT-FeCr, LSFNT-FeCr-ScYSZ and LSFNT-ScYSZ. Among these designs, LSFNT-FeCr-ScYSZ anode backbone showed the most promising microstructure with significantly improved adhesion with electrolyte and metal support (Figure 2b). The addition of small amount of ScYSZ improved the adhesion between the anode backbone and the electrolyte and the FeCr addition ensured adhesion with the metal support.

2.1.3 Integration of High Performance Cathodes

The cell design used in the project required that the cathode was sintered in-situ during the initial start-up and operation of the cell / stack. The in-situ “sintering” temperature was significantly lower than the temperature usually used for purely ceramic based intermediate and high temperature SOFCs. The effect of in-situ sintering temperature and time on the electronic conductivity, impedance and performance of various cathodes has been studied [8]. The different cathode materials, such as $(La_{0.6}Sr_{0.4})_{0.99}CoO_3$ (LSC) and $La_{0.58}Sr_{0.4}Co_{0.2}Fe_{0.8}O_3$ (LSCF) were investigated and compared in the temperature range of 650 – 950 ºC. In contrast to LSCF, the LSC-based

cathodes showed excellent sintering capabilities, electronic conductivity and performance. The polarization resistance (R_p) of the LSC based cathodes was 0.05 Ωcm^2 at 800 ^oC. which to our knowledge is the best performance reported in the literature for a few µm-thick, single layer, 800ºC in-situ sintered cathodes [13]. The drawback of LSC based cathodes was a relatively high thermal expansion coefficient (TEC) compared to other cell components. The challenge with this type of cathode materials was to make them mechanically robust towards thermal cycling. Efforts were made to address this issue by decreasing the cathode and current collecting layer (CCL) thickness down to a thin ~15 µm LSC layer, which was acting both as a cathode and CCL. Testing of such thin LSC cathodes on single cells (16 cm^2 active area) showed promising and reproducible results with no observable delamination. The same cathode layer was integrated on to the larger cells: 12 cm x 12 cm cells for Topsoe Fuel cell A/S (TOFC) stacks and 15.3 cm x 8.3 cm cells for ElringKlinger AG (EK) stacks. The conditioning and initial performance testing of such stacks did not show any damage of the cathode.

2.1.4 Advanced Cell Manufacturing Methods

Making the multilayered structures using tape casting process can be more cost-efficient if the layers can be cast simultaneously, particularly for mass production. During the course of the project, a co-casting process, where all the layers were casted simultaneously, was developed with different variations (wet-on-dry, semi wet-on-wet and wet-on-wet). Among these variations, the wet-on-dry and semi wet-on-wet were the most successful. It was demonstrated that the cell fabrication process can be up-scaled and more than 500 cells of different sizes with maximum cell area of > 400 cm^2 were fabricated. Furthermore, the flexibility of the cell fabrication process with respect to cell geometry was showed through the fabrication of cells with sizes ranging from 5 cm x 5 cm to 14.5 cm x 29 cm. Along with the scalability and flexibility, this process also showed reasonably high yield (>80%) of the cells per batch, which indicates that this process can be scalable and industrially relevant. In addition, the co-casting and co-sintering of different layers in the cells can make the cell fabrication process highly cost-effective.

2.2 Electrochemical Characterization

In order to complement the cell development process and to monitor the advancements made through the process variations and new cell components, the cells were continuously evaluated using electrochemical characterization tools. In the following, two MS-SOFC types (Type A and

Type B) were compared by current/voltage (CV) characteristics and electrochemical impedance spectra (EIS) - labeled in the following (Figure 3 and 5) as Type A with black lines/symbols and Type B with red lines/symbols. In the test bench, the single cells with an active electrode area of 1 cm² passed an identical initialization protocol before the actual characterization measurements. The relatively small active electrode area of 1 cm² together with the high gas flow rates (250 sccm) at anode/cathode ensure a homogeneous gas/temperature distribution. In this way, well-defined operating parameters can be secured during the CV/EIS-measurements. The results in Figure 3a show the measured CV-curves of both tested MS-SOFC types, whereby type A exhibited a superior performance. For the set operating conditions, the expected constant slope over the whole measured voltage range was observed for both cell types. Consequently, as shown in Figure 3b, the calculated total cell resistance (ASR_{total}) at j_{cell} = 0.5 Acm^{-2} was ~27% lower for cell type A compared to type B. However, these were initial performance results and do not include the durability contribution. In further experiments, MS-SOFCs of type A with the FeCr:YSZ anode design exhibited a strong degradation due to pronounced Cr_2O_3-scale formation in the AFL and throughout the anode backbone. Even under mild operating conditions (OCV, 650 °C, 20% humidified H_2), only initial performance measurements delivered reliable data. In contrast, cells with the LSFNT anode design (Type B, red) showed a much improved corrosion resistance, even in long term experiments (>2000 h) under polarization. Nevertheless, even the improved cell robustness was accompanied with a decrease in cell performance over time between 0.5 – 1.2 % per 100 h, depending on the water vapor content in the fuel gas. This is shown by Figure 4, where the resulting power density at j = 0.25 A cm^{-2} was recorded for two identical Type B cells, operated at T = 650 °C in low (only leakage) and elevated (20%) humidified H_2 as fuel gas. Similar electrochemical behavior for both Type A and Type B cells was observed for cells with larger active area (16 cm^2).

In order to unravel the underlying loss mechanisms, EIS were recorded in the frequency range between f = 3.5 MHz and 10 mHz by a Solartron 1260 frequency response analyzer. Example results are shown in Figure 5a in the Nyquist plot. Analyzing these EIS depicted in Figure 5a, the superior performance of cell Type A can be explained mainly by a lower serial resistance of type A compared to Type B, rather than by greater differences in the polarization resistance. By calculating the distribution of relaxation times (DRT) of each recorded EIS [14], a higher resolution of occurring loss processes can be achieved, which is shown in Figure 5b. Here, a higher sensitivity for Type B in the frequency range between f = 10-1000 Hz was observed, where the anode electrochemistry exhibits its dominant impact on the impedance for these MS-SOFC anodes. An

explanation for the superior serial resistance could be the better electronic conduction of FeCr metal particles compared to LSFNT.

With the help of an established, physical meaningful equivalent circuit model the occurring loss processes were evaluated and quantified. More details were described in [15]. Unfortunately, due to insufficient cell stability in case of Type A, the method could only be applied to Type B cell, as the change in polarization resistance during the whole measurement should not exceed 5% in order to maintain meaningful results in the complex nonlinear least squares (CNLS)-fitting process [16]. The determined losses for MS-SOFC type B are depicted in the Arrhenius-plot in Figure 6.

2.3 Coatings for Cell/Stack Components

Protective coatings were developed for the interconnect components for use in both anode and cathode sides. The coating process development was based on the pre-coated PVD process developed by Sandvik Materials Technology [17]. This roll-to-roll coating process allows for high volume production, which reduces cost. Development of Co nano coatings (~ 600nm) acted as a starting point for the cathode side coating development. Earlier investigations have shown that the coating was quickly converted into Co_3O_4, which formed a cap layer on the surface [18]. During exposure Mn from the steel diffuses outwards resulting in the formation of $(Co,Mn)_3O_4$. It has been shown that despite the low thickness, this coating effectively impedes Cr evaporation for more than 3000 h at 850 °C [18]. In order to improve high temperature oxidation resistance further, the use of the coatings based on Ce and La was investigated. It was observed that a 10 nm intermediate layer of Ce significantly reduced the oxide scale thickness [19-22]. This beneficial effect could also be confirmed in simulated anode gas (Ar-5%H_2-3%H_2O) [23].

A critical prerequisite for the pre-coated concept was that coated flat steel sheet can be stamped into an interconnect shape without impairing the protective properties of the coating. This was investigated on different substrates (Sanergy HT, Crofer APU and AISI 441) in combination with Co and Co/Ce coatings [24, 25]. The Cr evaporation rates of un-deformed material were compared with pre-coated material deformed in different ways. Deformation included Erichsen deep drawing cup tests as well as pressing into real interconnect shapes employing designs from TOFC and EK. SEM analysis of the deformed surfaces showed that the coating exhibits severe damage during deformation manifested by spalled areas and major cracks. However, upon high temperature exposure Co and Mn quickly diffuse into the damaged areas resulting in the formation of continuous $(Co,Mn)_3O_4$ layer (see Figure 7). A cross-section confirmed that a thin continuous

$(Co,Mn)_3O_4$ layer is already formed after 24h (see [25]). This corresponds well to the Cr evaporation measurements shown in Figure 8 for Crofer 22 APU coated with 600 nm Co or Co/Ce (600/10 nm). It was common for all the investigated samples (different interconnect designs, steel substrates) that no significant increase in Cr evaporation was recorded when comparing deformed to un-deformed samples, demonstrating a self- healing behavior of the coatings.

2.4 Modelling and Simulation

Different numerical models and simulation tools on various length scales, from micro to macro, were used for the analyses and investigation of the main losses and failure mechanisms in cells and stacks. This included the implementation and further development of electrochemical and thermo-mechanical models. The models were applied to investigate the loss and degradation mechanisms in cells and stacks. The identification and characterization of cell parameters, allowed for a proper evaluation of the cell performance, and offered the opportunity to assess the quality and reliability of the MS-SOFCs.

2.4.1 Cell and Repeat Unit Modelling

In order to classify the different MS-SOFC generations developed within the METSAPP project, an existing electrochemical model [15] was adopted, which was developed within the preceding METSOFC project for a similar MS-SOFCs architecture. By employing the in [15] described equivalent circuit in combination with a complex non-linear least square fit (CLNS) method, a separation and consequently the quantification of occurring loss processes can be realized. Furthermore, the achieved results allow a determination of cell inherent material parameters for a finite element method (FEM) modeling approach described below.

In order to pre-evaluate different stack designs, a 2D repeat unit (RPU) model framework has been developed based on the FEM, describing a 2D cross section perpendicular through a stack layer level. Due to symmetry reasons and assuming high gas flow rates, the RPU accounts for the whole stack layer level. The physical processes regarded in the model were: (i) electronic/ionic conduction in the porous electrodes, metallic interconnectors (MIC) and electrolyte (ii) electrochemical charge transfer at the electrode/electrolyte interfaces and (iii) gaseous species transport within the porous electrode microstructures. The model framework was parameterized with electrode kinetics and effective electrolyte / barrier layer conductivity data obtained from EIS measurements recorded on MS-SOFC Type B, anode microstructure data from 3D reconstruction and cathode electronic

conductivity from the literature [13], leaving the cathode microstructure as remaining unknown parameter. Therefore, data from a validated LSCF microstructure generator [26] was used as an approximation. In Figure 9, a comparison of measured and simulated C/V-curves are shown for three different temperatures at constant electrode partial pressures. The good agreement between measured and predicted data imply well determined electrode and electrolyte kinetics parameters.

2.4.2 Failure Modes Identification and Microstructural Modelling

In order to understand the failure mechanisms, relevant failure modes were identified for the MS-SOFCs. This was done with the help of AVL's Load Matrix™ methodology. The first part of this approach represents a "System Analysis", where all components of the MS-SOFC-stack were screened for reliability-relevant failure modes. In addition, a prioritization of the listed failure modes was performed. The prioritization states how relevant a failure mode was for the stack validation. 10 identified failure mechanisms were transferred into an effective long term test program.

One identified major failure mode, unique to MS-SOFCs, was the oxidation of the metal-support and the AFL. In order to study its influence on the cell-performance, a 3-D microstructural model of the metal-support was set-up. The measurement of the metal-support microstructure was carried out with X-ray computed tomography and the reconstructed measurement was converted into a computational geometry representing the pores of the metal-support. A 3-D diffusion model, implemented in OpenFOAM®, allowed for the evaluation of mass-transfer related losses [27].

Furthermore, a sophisticated oxidation model was developed for the metal-support and the AFL, to study its effects on the diffusion processes. The impact of oxidation on the metal-support was analyzed on the micro-meter scale by implementing a mathematical model that describes the growth of the oxide scale as a function of time (Figure 10). The decreasing pore size, due to oxidation, impedes gas diffusion, which in turn increases the mass-transport related losses of the MS-SOFC [28].

This knowledge helped to understand the impact of oxide scale thickness on the mass-transport and metal-support stability, and long-term simulation studies of the mass-transport related performance enhanced the knowledge-gain of short-term testing.

2.5 Stack Development and Testing

The stack development and testing activities were carried out by two different partners in the consortium, initially by TOFC and after their exit from the project consortium, by EK. In order to build a successful stack, TOFC explored the sealing methods, e.g. laser welding; cathode sintering methods e.g. in-situ and/or ex-situ sintering, stack composition and conditioning treatments along with mathematical models for stack designing. With the introduction of a "double-weld" together with improved laser weld parameters, the leak rates from the cell-interconnect component became sufficiently low for proper implementation into stacks. An *in-situ* cathode sintering procedure was developed, where the cathode was sintered when the stack has been assembled and sealed with glass at elevated temperatures. The procedure required testing and implementation of new glass materials for sealing and new methods for their application and processing (heat treatment and compression). The stack treatments included variations in the application and duration of compression forces, in order to determine the importance of mechanical force and metal creep. The conclusion from those tests and others was that too little load adversely affected stack start-up, whereas higher loads could be tolerated in some cases without catastrophic failure.

The progress achieved in different activities mentioned above resulted in improvements on all aspects of the stack fabrication steps and conditioning and different modelling & simulation tools for stack design optimization, which lead to the development of promising stacks at TOFC (Figure 11a). The stack was unfortunately never characterized in a stack test due to the closing of TOFC at the time this stack was produced. Subsequently, EK continued the stack development and testing activities albeit with a different stack design. The different stack design at EK necessitated repeated investigation of sealing process, where different configurations of laser welding the cell with cell frame were investigated and suitable configuration was identified (Figure 11b). Two 5-cell stacks were built at EK (Figure 11c) and after stack conditioning some leaks were observed, indicating further optimization of the sealing process is required. Nevertheless, it was demonstrated that the MS-SOFCs developed in METSAPP project can be integrated into different stack designs.

3. Conclusions

The efforts to mature the MS-SOFC technology were continued in the EU METSAPP project, mainly addressing the development of robust cells and stacks. MS-SOFCs with novel AFL designs based on doped-$SrTiO_3$ were successfully elaborated, which showed promising electrochemical performance, reasonable stability and oxidation resistance in varying test conditions. A scalable and environmentally friendly cell manufacturing process for mass production of cells was established.

More than 500 cells of different sizes with maximum cell area of >400 cm^2 were fabricated. Numerical models were developed to identify different degradation mechanisms, in particular the metal particle oxidation in metal support and anode backbone. Protective coatings for the interconnects that can reduce the Cr evaporation by 90% and the Cr_2O_3 scale thickness by 3 times were obtained. It was demonstrated that the MS-SOFCs developed in METSAPP project can be integrated into two radically different stack designs. Further improvement of oxidation resistant anodes is necessary for the commercialization of the metal supported SOFC technology.

Acknowledgements

Financial support by the EU project METSAPP (FP7-278257) and Energinet.dk under the project ForskEL 2012-1-10806 is gratefully acknowledged. The authors also would like to thank Dr. Peter Blennow, Dr. Niels Christiansen for their contribution to the project in different capacities.

References:

[1] M.C. Tucker, *J. Power Sources* **2010**, *195*, 4570.

[2] P. Blennow, J. Hjelm, T. Klemensø, S. Ramousse, A. Kromp, A. Leonide, A. Weber, *J. Power Sources* **2011**, *196*, 7117.

[3] M. Brandner, M. Bram, J. Froitzheim, H.P. Buchkremer and D. Stoever, *Solid State Ionics* **2008**, *179*, 1501.

[4] P. Blennow, J. Hjelm, T. Klemensø, Å. H. Persson, K. Broadersen, A.K. Srivastava, H. L. Frandsen, M. Lundburg, S. Ramousse and M. Mogensen, *ECS Trans.* **2009**, *25,* 701.

[5] T. Klemensø, J. Nielsen, P. Blennow, ÅH. Persson, T. Stegk, B.H. Christensen, S. Sønderby, *J. Power Sources* **2011**, *196,* 9459.

[6] J. Nielsen, T. Klemensø, P. Blennow, *J. Power Sources* **2012**, *219,* 305.

[7] B. J. McKenna, N. Christiansen, R. Schauperl, P. Prenninger, J. Nielsen, P. Blennow, T. Klemensø, S. Ramousse, A. Kromp and A. Weber, *Fuel Cells* **2013**, *13,* 592.

[8] P. Blennow, J. Hjelm, T. Klemensø, ÅH. Persson, S. Ramousse, M. Mogensen, *Fuel Cells* **2011**, *11,* 661

[9] R. Knibbe, H.-. Wang, P. Blennow, K. Thydén, ÅH. Persson, L. Mikkelsen, T. Klemensø, *J. Power Sources* **2013**, *228, 75*

[10] P. Blennow, B. R. Sudireddy, Å. H. Persson, J. Nielsen, R. Sachitanand, J. Froitzheim, *ECS Trans.* **2013**, *57*, 771.

[11] P. Blennow, B.R. Sudireddy, ÅH. Persson, T. Klemensø, J. Nielsen, K. Thydén, *Fuel Cells* **2013**, *13*, 494.

[12] D. Neagu, G. Tsekouras, D. N. Miller, H. Ménard, J.T.S. Irvine, *Nature Chem.* **2013**, *5*, 916.

[13] J. Nielsen, P. Hjalmarsson, M. H. Hansen, P. Blennow, *J.Power Sources* **2014**, *245*, 418.

[14] V. Sonn, A. Leonide and E. Ivers-Tiffée, *J. Electrochem. Soc.* **2008**, *155*, B675.

[15] A. Kromp, J. Nielsen, P. Blennow, T. Klemenso and A. Weber, *Fuel Cells* **2013**, *13*, 598.

[16] H. Schichlein, A. C. Müller, M. Voigts, A. Krügel and E. Ivers-Tiffée, *J. Appl. Electrochem.* **2002**, *32*, 875.

[17] Pre-coated PVD process technology, can be found under http://smt.sandvik.com/en/products/strip-steel/strip-products/coated-strip-steel/production-process/

[18] J. Froitzheim, S. Canovic, M. Nikumaa, R. Sachitanand, L.G. Johansson, J.E. Svensson, *J. Power Sources* **2012**, *220*, 217.

[19] S. Canovic, J. Froitzheim, R. Sachitanand, M. Nikumaa, M. Halvarsson, L.G. Johansson, J.E. Svensson, *Surf. Coat. Techol.* **2013**, *215*, 62.

[20] J. Froitzheim, A. Magraso, T. Holt, M.W. Lundberg, H.F. Windisch, R. Berger, R. Sachitanand, J. Westlinder, J.E. Svensson, R. Haugsrud, *ECS Trans.* **2013**, *57*, 2187.

[21] J. Froitzheim, J.E. Svensson, *ECS Trans.* **2011**, *35*, 2503.

[22] J.G. Grolig, J. Froitzheim, J.E. Svensson, *J. Power Sources* **2014**, *248*, 1007.

[23] R. Sachitanand, M. Sattari, J.E. Svensson, J. Froitzheim, *Fuel Cells* **2016**, *16*, 32.

[24] H. Falk-Windisch, I. Mertzidis, J.E. Svensson, J. Froitzheim, *ECS Trans.* **2015**, *223*, 1617.

[25] H. Falk-Windisch, M. Sattari, J.E. Svensson, J. Froitzheim, *J. Power Sources* **2015**, *297*, 217.

[26] A. Messner, J. Joos, M. Ender, A. Weber, E. Ivers-Tiffée, Proc. *11th European SOFC and SOE Forum, Lucerne*, Switzerland, **2014**, pp. B0814.

[27] G. Reiss, H. L. Frandsen, W. Brandstätter, A. Weber, *J. Power Sources* **2015**, *273*, 1006.

[28] G. Reiss, H. L. Frandsen, Å. H. Persson, C. Weiß, W. Brandstätter, *J. Power Sources* **2015**, *297*, 388.

Figure Captions:

Figure 1: Examples of various coatings showing overview and detail of: (a) metal support with surface contamination of silicon (dark region between the coating and the metal); (b) clean metal support; (c) coating in the anode functional layer.

Figure 2: Metal supported half-cell with (a) STN-FeCr anode backbone (b) SEM cross-section of the LSFNT-FeCr anode backbone based half-cell.

Figure 3: a) Current-voltage characteristics recorded on MS-SOFCs with Type A (black) and Type B (red) anode designs. b) Total area specific resistance comparison at $j_{cell} = 0.5$ Acm^{-2}. Operating conditions: T = 700 °C, 20% humidified H_2 as fuel and ambient air as oxidant.

Figure 4: Performance of two Type B cells under the load (0.25 Acm^{-2}) for ~1000h with different water vapor amounts in the fuel gas.

Figure 5: (a) EIS recorded on MS-SOFCs with Type A (black) and Type B (red) anode designs. (b) Corresponding DRT curves calculated from (a) Operating conditions: T = 700 °C, 20% humidified H_2 as fuel and ambient air as oxidant.

Figure 6: Arrhenius-plot with CNLS-fitting determined losses of type B MS-SOFC.

Figure 7: Surface of a pre coated steel (600 nm Co coated Crofer APU) stamped into an interconnect. The imaged areas represent the most severely damaged part of the interconnect after different exposure times (850 °C). It can be seen that initially large areas of the coating are missing (black areas in Co map). During exposure, Co diffused into the damaged areas resulting in a continuous outer Co rich oxide.

Figure 8: Accumulated Cr vaporization as a function of time at 850 °C in air 3% H_2O. Uncoated undeformed Crofer 22 APU (grey squares) exhibits approximately ten times higher evaporation than all coated samples. These include: 600 nm Co coated undeformed (open squares), Crofer 22 APU pressed into interconnect and subsequently coated with 600 nm Co (circles), 600 nm Co pre-

coated Crofer 22 APU subsequently pressed into interconnect (triangles), 600 nm Co + 10nm Ce pre-coated Crofer 22 APU subsequently pressed into interconnect (stars).

Figure 9: Comparison of measured (lines) and simulated (symbols) C/V-curves at three different temperatures and constant electrode partial pressures.

Figure 10: 3D regenerated metallic support microstructure with corrosion layer (left hand side). The right-hand picture shows one slice through the geometry with corroded pores (red indicating fully corroded areas, while blue regions correspond to open pore space).

Figure 11: (a) A 10-cell TOFC stack, (b) Microstructure of the welding seam along the outline of a cell and cell frame (top cell / bottom cell frame) and (c) a 5 cell EK stack. Both (a) and (c) are after assembly and conditioning with in-situ sintering of the cathode.

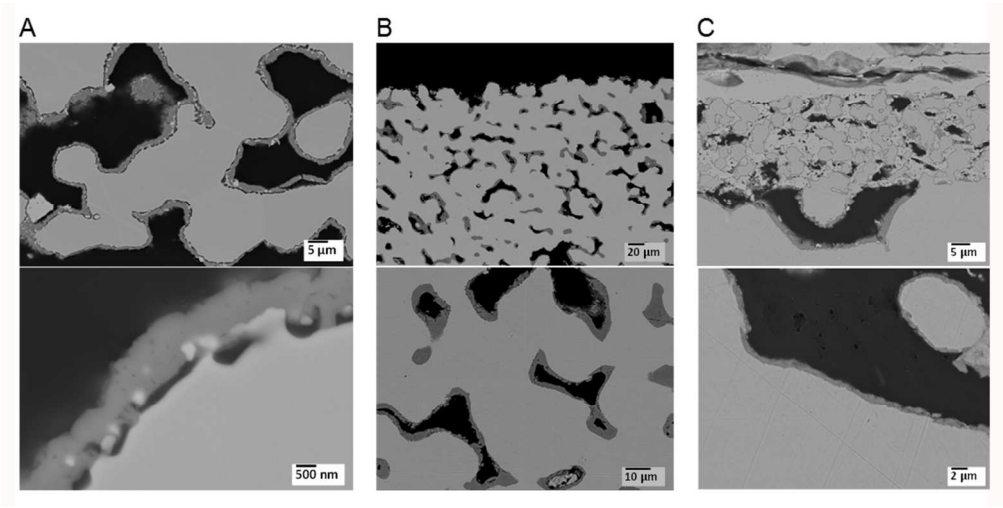

Figure 1

165x82mm (300 x 300 DPI)

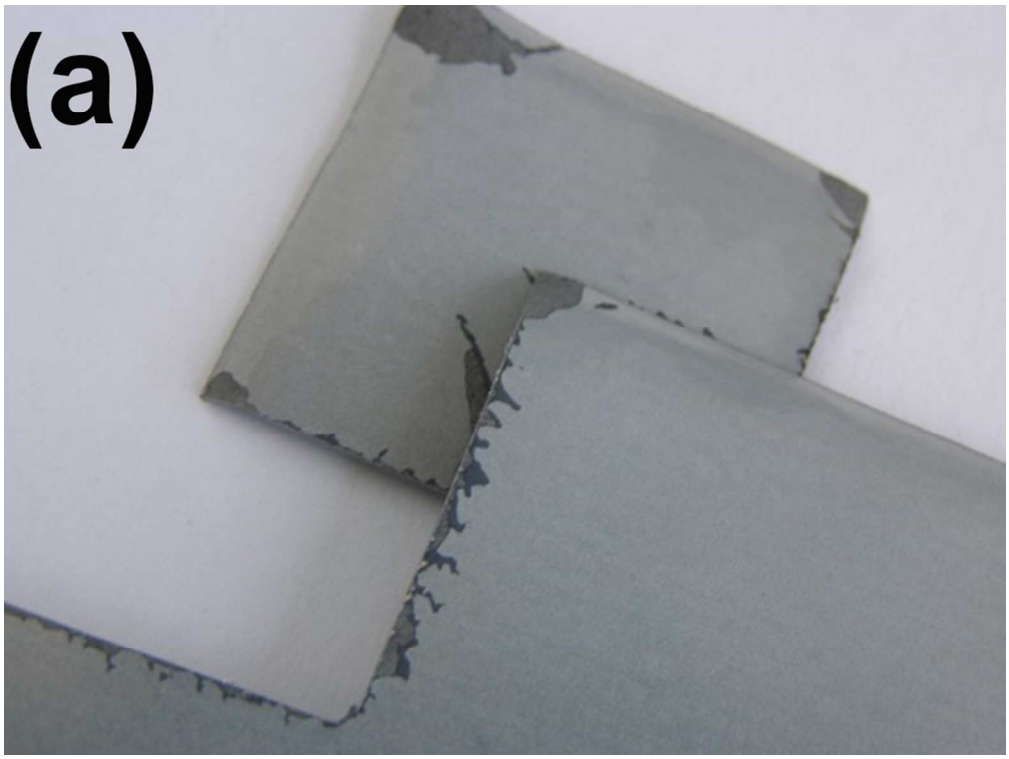

Figure 2a

85x63mm (300 x 300 DPI)

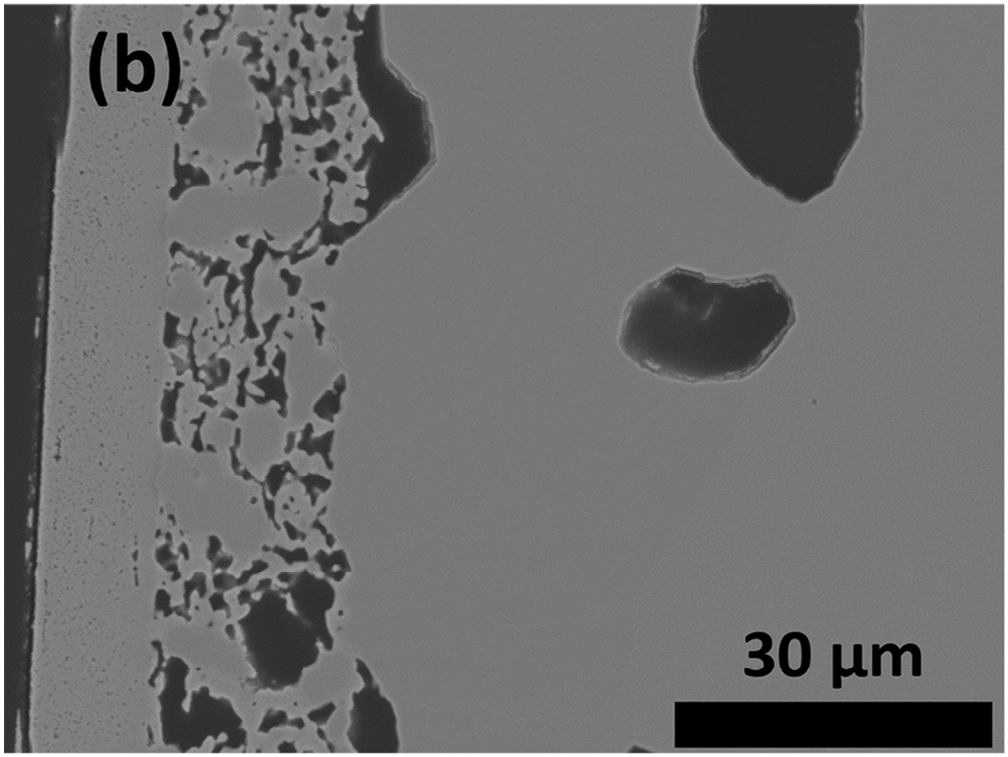

Figure 2b

85x65mm (300 x 300 DPI)

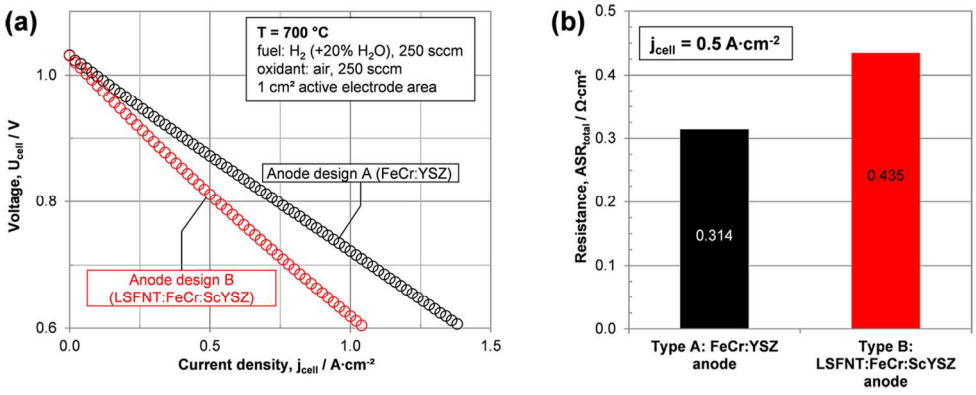

Figure 3

170x67mm (300 x 300 DPI)

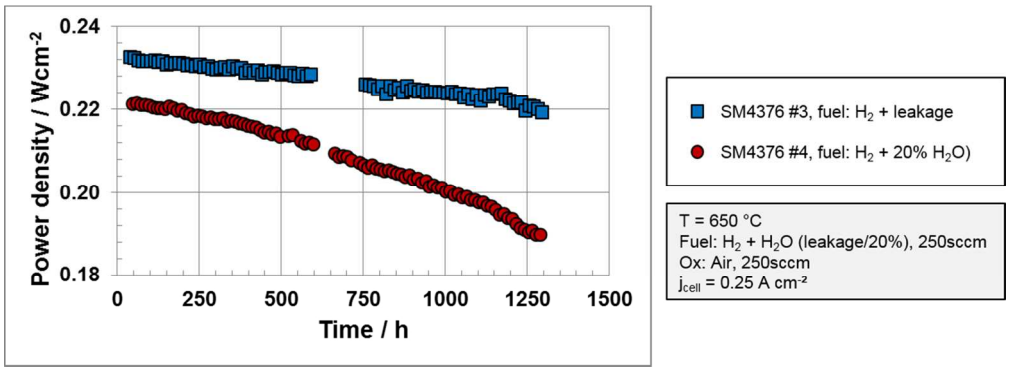

Figure 4

170x61mm (300 x 300 DPI)

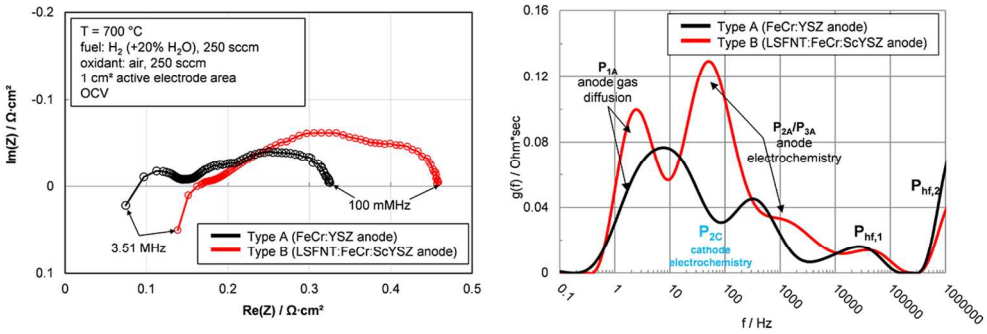

Figure 5

170x58mm (300 x 300 DPI)

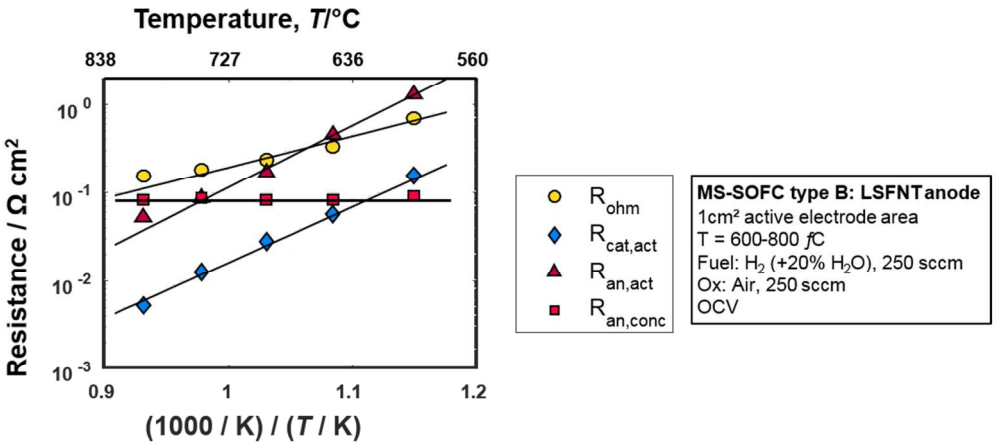

Figure 6

170x78mm (300 x 300 DPI)

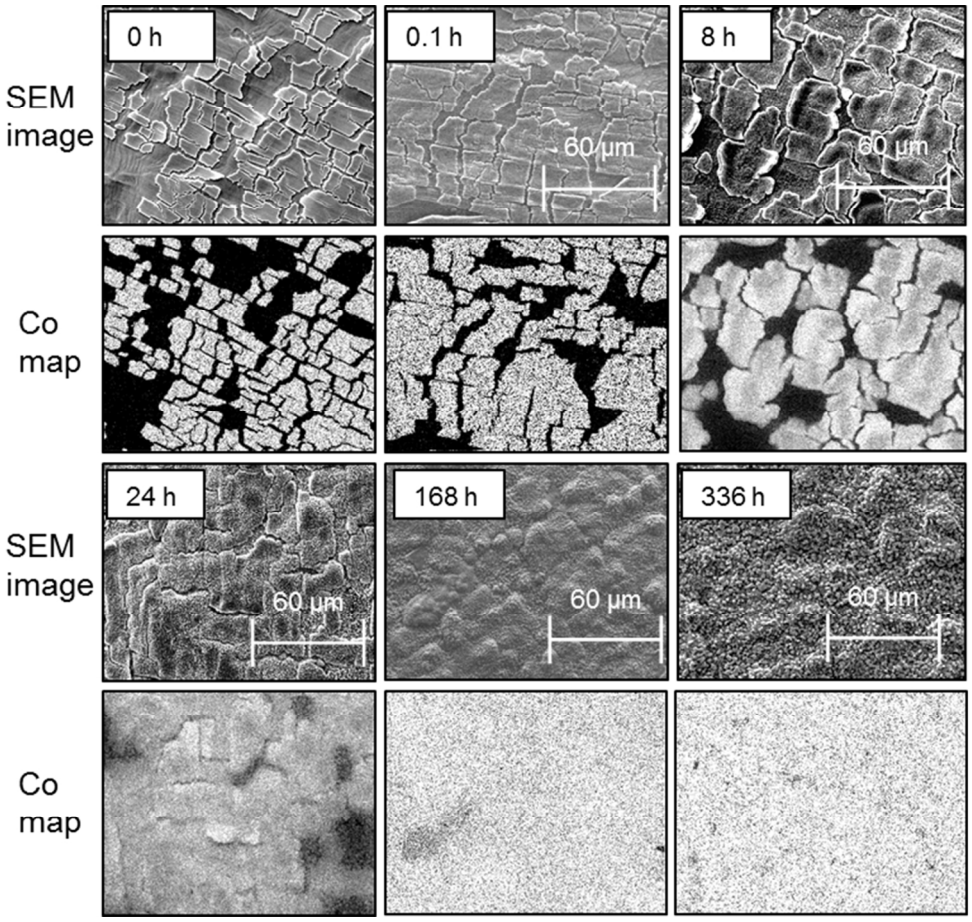

Figure 7

134x122mm (300 x 300 DPI)

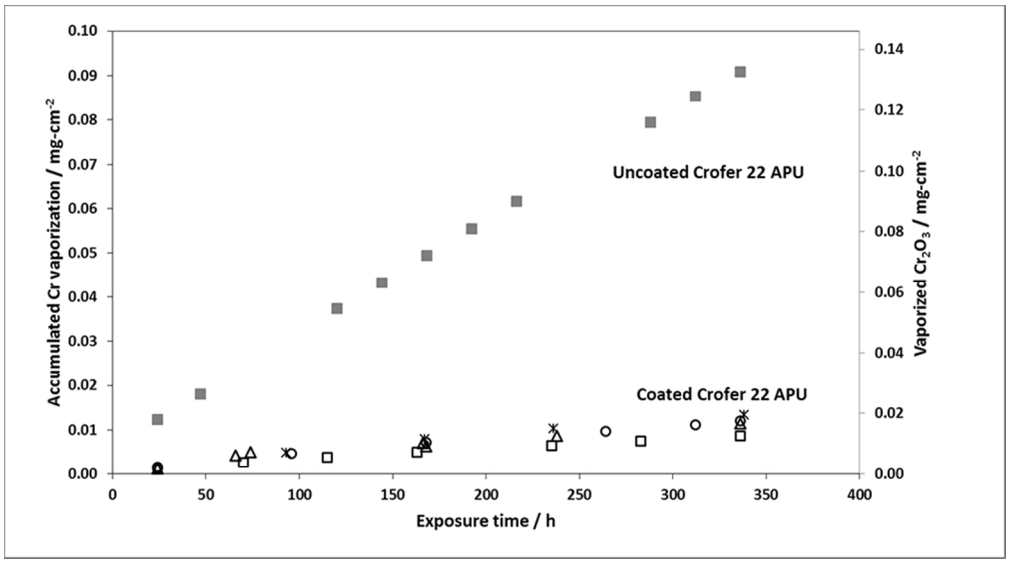

Figure 8

85x46mm (300 x 300 DPI)

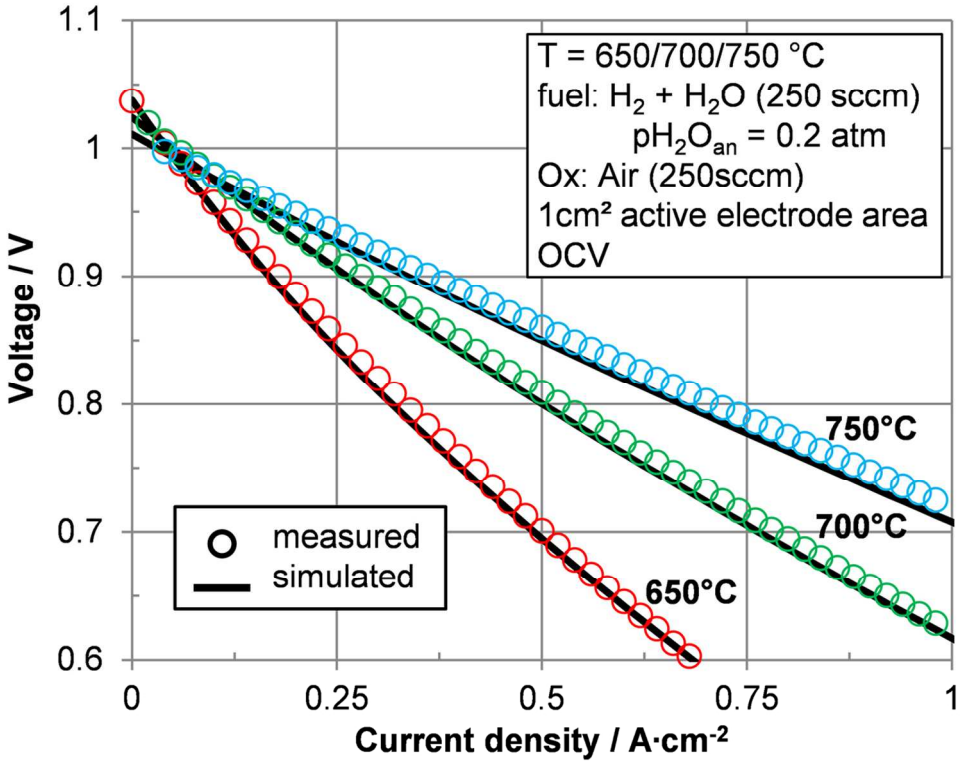

Figure 9

119x93mm (300 x 300 DPI)

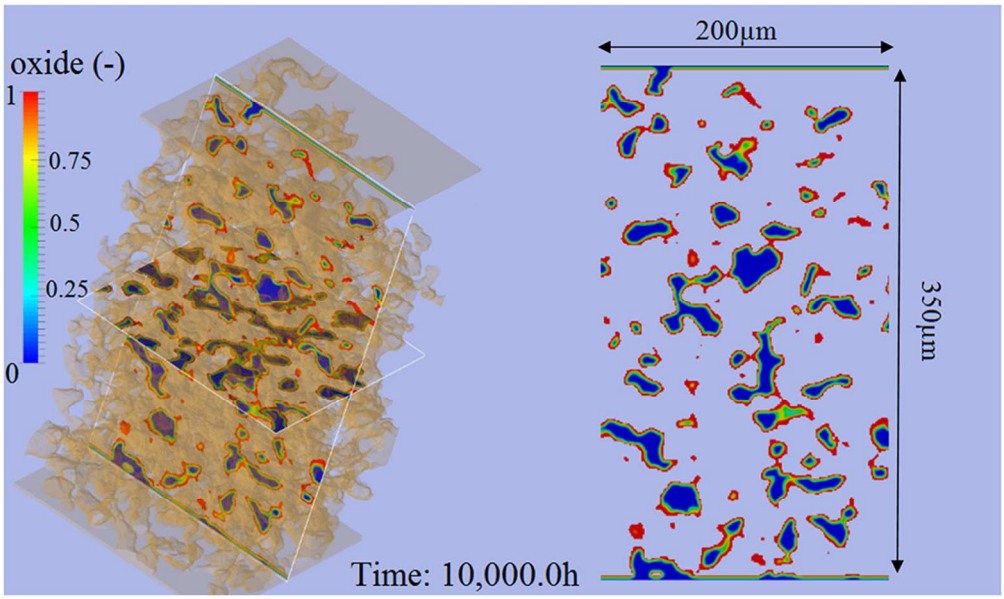

Figure 10

90x53mm (300 x 300 DPI)

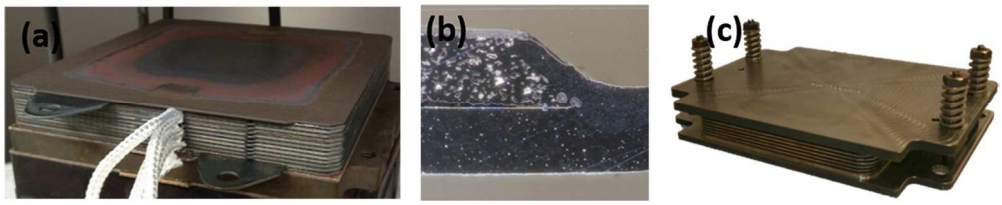

Figure 11

170x34mm (300 x 300 DPI)